Applied Mathematics & Information Sciences
An International Journal

http://dx.doi.org/10.18576/amis/180118

Numerical solution of MHD Micropolar Casson fluid flow over Porous linearly stretching sheet with heat source / sink

Pravendra Kumar [1], *Bhupander Singh* [1,*], *Seema Goyal* [1], *Kapil Kumar* [1], *Aajy Nandan* [1], *Kottakkaran Sooppy Nisar* [2], *Shawkat Alkhazaleh* [3] *and Abdel-Haleem Abdel-Aty* [4]

[1] Department of Mathematics, Meerut College, Meerut-250003, Uttar Pradesh, India
[2] Department of Mathematics, College of Science and Humanities in Alkharj, Prince Sattam Bin Abdulaziz University, Alkharj 11942, Saudi Arabia
[3] Department of Mathematics, Faculty of Sciences and Information Technology, Jadara University, Irbid, Jordan
[4] Department of Physics, College of Sciences, University of Bisha, Bisha 61922, Saudi Arabia

Received: 12 Aug. 2023, Revised: 18 Dec. 2023, Accepted: 22 Dec. 2023
Published online: 1 Jan. 2024

Abstract: In the current investigation, we obtain the numerical solution of MHD Micropolar Casson fluid flow over linearly stretching sheet with heat source / sink effect in porous medium. Through the implementation of appropriate similarity transformations, the governing partial differential equations are converted into nonlinear ordinary differential equations. These equations are subsequently numerically solved via the utilization of MATLAB software, resulting in the derivation of numerical solutions for the aforementioned transformed nonlinear ordinary differential equations. The obtained numerical answer velocity of fluid, temperature and micro-rotation are presented in graphical form, wherein the impact of numerous relevant factors, for instance the Casson fluid parameter, porosity parameter, magnetic parameter, micro-inertia density parameter, micro-coupling parameter, heat generation parameter, etc., on the micro-rotation, velocity and temperature profiles are thoroughly analyzed and spoke about. The graphical depictions of the resulting data are expounded upon in detail.

Keywords: Micropolar fluid; Casson fluid; Magnetohydrodynamic; Porous medium; linearly stretching sheet.

1 Introduction

Micropolar fluids refer to fluids that contain microstructures. These fluids consist of rigid particles that are oriented at random and drowned in a sticky medium. The applications of micropolar fluids are vast and include polymers, foodstuffs, blood, alloys and liquid metal, plasma as well as drilling for gas and oil. Such fluids are characterized by non-symmetric stress tensors. Eringen [1, 2] provided explanations from theory for micropolar fluids and identified the impact of micro motion of fluid elements. He offered a rational and important summary of the standard Navier–Stokes model, which covers many more phenomena in compared to the classical model, theory and applications. Furthermore, his generalization had a good structure and wasn't unduly complicated. According to Borrelli et al. [3], micropolar fluids have a variety of uses in the pharmaceutical, chemical, engineering, and food industries. Alkasasbeh [4] numerical solved the nonlinear partial differential equation for MHD flow of micropolar Casson fluid through a circular object that is horizontal and investigated the impacts of different parameters based on flow characteristics and heat transfer coefficients. Pramanik [5] has conducted extensive research on the phenomenon of heat flow during suctioning or blowing at surfaces. Saidulu and Venkata Lakshmi [6] have adequately investigated the subject of heat transmission with slip effects of Casson. Shu [7] obtained new fundamental solutions for micropolar fluids, which are useful for solving microscale flow problems involving rheologically complex fluids. Passos et al. [8] numerically studied the direction a Casson liquid through a flow-disturbing rib in a rectangular $\mu-$channel and investigated non-Newtonian behavior's impact on fluid

* Corresponding author e-mail: bhupandersingh1969@gmail.com

flow properties. In their study, Hegab and Liu [9] employed a mathematical model grounded on the micropolar fluid theory to scrutinize the flow characteristics in micro orifices. Their findings evinced that the micropolar fluid theory affords a superior close-up of the observed escalation friction in micro channel flows. Mitarai et al. [10] demonstrated that the utilization of a micropolar fluid model effectively characterizes collisional granular flows on an incline. This approach offers a hydrodynamical framework that is well-suited for granular systems. Mohana Ramana et al. [11] conducted comprehensive numerical analysis of the steady MHD stagnation point flow of a Casson fluid through a stretching sheet by a heat source and chemical reaction. The authors took into account various slip boundary conditions and viscous dissolution phenomena to better comprehend the problem at hand. An examination of the radiation effects of MHD Casson fluid flow through an exponentially extending sheet that was imbedded in a porous medium was done by Reddy et al. [12]. The study also analyzed the role of slip effects and heat source/sink. Asifa et al. [13] conducted an investigation into the unsteady flow of Casson fluid in a porous medium, subjected to thermal radiation, magnetic field, and heat source/sink, between two heated walls. Saif Ur Rehman et al. [14] conducted a study in which they analyzed the effect of buoyancy parameters and radiation on the phenomenon of MHD micropolar nano fluid flow beyond a stretching /shrinking surface. Dey et al. [15] investigated the transfer of mass and energy on a porous surface using magnetohydrodynamic fluid. Saidulu and Reddy [16] performed research into the effects of dissipation on heat and mass transportation by analyzing the micropolar flow on a stretchable surface, which is comparable in nature. Their final statement implies that the growth in magnitude of the Eckert number results in an upsurge in the temperature curve, whereas the concentration curve declines as the Schmidt number increases. Nandeppanavar et al. [17] conducted an investigation on the characteristics of unsteady On an elongating medium, the Casson fluid flows with a focus on examining the heat transfer phenomena through dissipation of viscosity. The utilization of thermal radiation has been widely recognized in numerous technological and industrial applications, including, but not limited to, natural gas, solar systems, nuclear reactors, gas turbine plants, energy production, astronomical processes, and communication satellites. Thermal radiation is an essential component of the energy conversion process, and its effects are radiated from both the working fluid and the heated wall. Its significance in the process of flow and heat transfer is critical, particularly in the development various energy conversion devices that operate at higher temperatures. Siegel and Howell [18] introduced a thermal radiation-based system that is driven by the interplay between the working fluid and the wall's emission properties. Salahuddin and Awais [19] conducted a study to investigate the impact of thermal radiation on the flow analysis of non-Newtonian fluid on a sensory surface. Their research revealed that the temperature curve is heightened by thermal radiation. Additionally, a significant investigation was carried out by Jalili et al. [20] with the objective of analyzing the thermal implications of nanofluid flow within the interplate region.

The discipline of magnetohydrodynamics (MHD) is concerned with investigation of the behavior of electrically conductive solutions when a magnetic field is present, a phenomenon which holds important significance in various manufacturing and technical applications, including but not limited to MHD generators, nuclear reactor design, and flow meters. Through a myriad of innovative research endeavors, it has been established that the application of a magnetic field has a profound influence on the transport and heat transfer properties of typical electrically conductive flows. The study of magnetohydrodynamics bears noteworthy implications, such as the utilization of liquid sodium for cooling nuclear power plants and the adoption of measuring induction pressure, which relies on fluid potential differences perpendicular to motion and the magnetic field, among other factors as suggested by Ganesan and Palani [21]. In relation to heat transfer in a magnetohydrodynamic stagnation point flow of the Cross fluid model towards a stretched surface, Hayat et al. [22] performed a research project of numerical simulation. An analysis on the dynamic and thermal boundary layers was carried out by Djebali et al. [23] in their study. The implementation of similarity solutions was used to investigate the subsequent development of these layers with a vertical flat plate. Warke et al. [24] conducted a thorough examination of the mathematical analysis pertaining to the stagnation point flow of radiative magnetomicropolar liquid that is observed passing through a stretching sheet. Swain et al. [25] investigated consequences of utilizing hybrid nanoparticles composed of multi-walled carbon nanotubes (MWCNT) and iron oxide (Fe3O4) on an exponentially porous shrinking sheet that exhibits chemical reaction and slip boundaries. Iqbal et al. [26] undertook an examination of the ramifications considering a magnetic field that is inclined on a stretching layer of micropolar-Casson fluid, while simultaneously considering the influences of viscous dissipation. The matter of micropolar-Casson fluid flow through a stretching surface was addressed by Kasim et al. [27] who were able to obtain a numerical solution. In the interim, Shah et al. [28] conducted an investigation on the effectiveness of heat transfer in an electrically conductive MHD flow of a Casson ferrofluid over a stretching sheet. The study by Alkasasbeh et al. [29] focused on the analysis of steady two-dimensional laminar magnetohydrodynamic (MHD) natural convection flow through a solid sphere that is immersed in a micropolar-Casson fluid in suspension. The study conducted by Jusoh et al. [30] investigated the problem of

mixed convection related to the Casson micropolar fluid over a surface that is either stretching or shrinking.

2 Mathematical model

In a porous media with permeability K, we consider the steady flow of a micropolar Casson fluid in two dimensions over a horizontal linear stretching sheet. A uniform transverse magnetic field B_0 is present, and this causes the fluid to conduct electricity. The induced magnetic field is negligible. Consider external flow is $u_e(x) = ax$ and the velocity of the stretching sheet is $u_w(x) = cx$, where a, c are positive constant and x is the coordinate considered together the stretching sheet. We assumed that both T_w and T_∞ are the melting and free stream temperature of the fluid respectively, where $T_w > T_\infty$ The modeling of the problem shown in figure 1

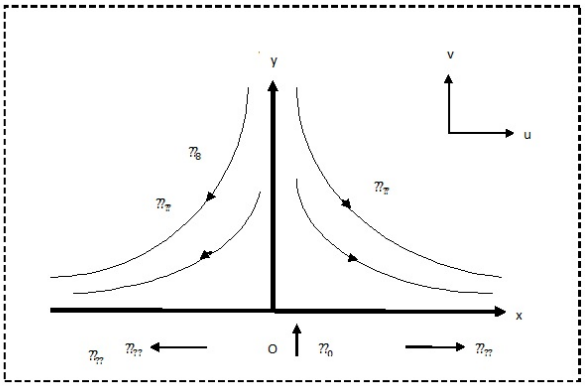

Fig. 1

The rheological equation describing the behavior of the Casson fluid is formulated as follows.

$$T_{ij} = \begin{cases} 2\left(\mu_B + \frac{P_y}{\sqrt{2\pi}}\right) e_{ij}, & \pi > \pi_c \\ 2\left(\mu_B + \frac{P_y}{\sqrt{2\pi_c}}\right) e_{ij}, & \pi > \pi_c \end{cases} \tag{1}$$

Where μ_B plastic dynamic viscosity, $\pi = e_{ij}e_{ij}$ and e_{ij} is the $(i,j)^{th}$ component of deformation rate, π denotes deformation rate, π_c is a critical value of non Newtoniam model, P_y is the yield stress of fluid. The equations that determine the system's behavior are derived under the aforementioned assumptions.

$$\frac{\partial u}{\partial x} + \frac{\partial v}{\partial y} = 0 \tag{2}$$

$$u\frac{\partial u}{\partial x} + v\frac{\partial u}{\partial y} = v\left(1 + \frac{1}{\beta}\right)\frac{\partial^2 u}{\partial y^2} - \frac{\sigma B_\circ^2 u}{\rho_f} + \left(\frac{\kappa}{\rho}\right)\frac{\partial N}{\partial y} - \frac{v}{K*\rho}\mu \tag{3}$$

$$u\frac{\partial N}{\partial x} + v\frac{\partial N}{\partial y} = \frac{\gamma}{\rho_j}\frac{\partial^2 N}{\partial y^2} - \frac{\kappa}{\rho_j}\left(2N + \frac{\partial u}{\partial y}\right) \tag{4}$$

$$u\frac{\partial T}{\partial x} + v\frac{\partial T}{\partial y} = \alpha\frac{\partial^2 T}{\partial y^2} - \frac{1}{\rho C_p}\frac{\partial q_r}{\partial y} + \frac{Q}{\rho C_p}(T - T_\infty) \tag{5}$$

Consider the boundary conditions pertaining to equations (2), (3), (4) and (5) as follows.

$$\begin{aligned} u &= u_w(x) = cx, T = T_w, N = 0, \quad \text{at} \quad y = 0 \\ u &\to u_e(x) = ax, T \to T_\infty, \quad \text{as} \quad y \to \infty \end{aligned} \tag{6}$$

Here α the thermal diffusivity of the fluid, β Casson fluid parameter, (u,v) =velocity components along axes, K permeability of the medium, k thermal conductivity, σ electrical conductivity of fluid, ρ the density of fluid q_r Radiative heat flux, κ micropolar fluid constant and C_p the specific heat at constant pressure.
Under the Rosseland approximation [31], the flux of Radiative heat may be expressed.

$$q_r = -\frac{4\sigma^*}{3k^*}\frac{\partial T^4}{\partial y} \tag{7}$$

Where σ^* is the Stefan-Boltzman constant and k^* is the mean absorption coefficient further, we presume that the temperature difference within the stream is such that T^4 is uttered as a linear function of temperature. Hence expanding T^4 in Taylor series about T_∞ and neglecting higher order terms, we obtain

$$T^4 \cong 4T_\infty^3 T - 3T_\infty^3$$

Similarity variables

$$\begin{aligned} \eta &= y\sqrt{\frac{a}{v}}, & \psi &= \sqrt{av}xf(\eta), \\ N &= a\sqrt{\frac{a}{v}}xg(\eta), & \theta(\eta) &= \frac{T - T_\infty}{T_w - T_\infty}, \end{aligned} \tag{8}$$

Where ψ denotes the stream function, its definition is such that $u = \frac{\partial \psi}{\partial y}$ and $v = -\frac{\partial \psi}{\partial x}$ are automatically in compliance with the continuity Equation (1). Through the utilization of this definition, we are able to acquire

$$u = axf'(\eta), v = -\sqrt{av}f(\eta) \tag{9}$$

Substitute Equations (8) & (9) into Equations (2), (3), (4) and (5), the transformed equations are

$$\left(1 + \frac{1}{\beta}\right)f'''(\eta) + f(\eta)f''(\eta) - f'(\eta)^2 - (M + \Omega)f'(\eta) + A_1 g'(\eta) = 0 \tag{10}$$

$$\lambda_0 g''(\eta) + f(\eta)g'(\eta) - f'(\eta)g(\eta) - A_1 B\left(2g(\eta) + f''(\eta)\right) = 0 \tag{11}$$

$$f(\eta)\theta'(\eta)+\left(R+\frac{1}{Pr}\right)\theta''(\eta)+\Delta\theta(\eta)=0 \quad (12)$$

The boundary conditions that correspond to similarity variables are presented herein.

$$f'(0)=\varepsilon,\ \ \theta(0)=0,\ \ g(0)=0 \quad \text{at} \quad y=0 \quad (13)$$

$$f'(\infty)\to 1,\ \ \theta(\infty)\to 1,\ \ g(\infty)\to 0 \quad \text{at} \quad y\to\infty \quad (14)$$

$$A_1=\frac{K}{\nu\rho},\quad M=\frac{\sigma B_o^2}{a\rho},\quad \lambda_o=\frac{\gamma}{\nu\rho},\quad B=\frac{\nu}{a},$$
$$\Omega=\frac{\nu}{aK},\quad P_r=\frac{\nu}{\alpha},\quad \Delta=\frac{Q}{a\rho C_p},\ R=\frac{16\sigma^* T_\infty^3}{3K^* K}$$

Where the primes denotes differentiation with respect to η, $M=\frac{\sigma B_o^2}{a\rho}$ magnetic parameter, $R=\frac{16\sigma^* T_\infty^3}{3K^* K}$ radiation parameter, $\Omega=\frac{\nu}{aK}$ permeability parameter, $P_r=\frac{\nu}{\alpha}$ Prandtl number, $\Delta=\frac{Q}{a\rho C_p}$ heat generation parameter, $\varepsilon=c/a$ stretching parameter, $\lambda_o=\frac{\gamma}{\nu\rho}$ spin gradient viscosity parameter, $B=\frac{\nu}{a}$ mico-inertia density parameter, $A_1=\frac{K}{\nu\rho}$ micro-coupling parameter and β Casson fluid parameter.
The two fundamental physical quantities under consideration are the skin friction coefficient denoted by C_f and the local Nussselt number denoted by Nu_x.

$$C_f=\frac{\tau_w}{\rho u_e^2}, Nu_x=\frac{xq_w}{k(T_\infty-T_w)}, \quad (15)$$

Where $\tau_w=\mu\left(1+\frac{1}{\beta}\right)\left(\frac{\partial u}{\partial y}\right)_{y=0}$ is surface shear stress, μ is dynamic viscosity of fluid, and $q_w=-k\left(\frac{\partial T}{\partial y}\right)_{y=0}+q_r$ is surface heat flux.
By means of the equation (9), one can determine the skin friction coefficient.

$$C_f=\frac{\tau_w}{\rho u_e^2}\ \Rightarrow\ Re_x^{1/2}C_f=\left(1+\frac{1}{\beta}\right)f''(0), \quad (16)$$

And the Nusselt number is

$$Nu_x=\frac{xq_w}{k(T_\infty-T_w)}\Rightarrow Re_x^{-1/2}Nu_x=-(1+R)\theta'(0), \quad (17)$$

Where $Re_x=\frac{u_e x}{\nu}$ represent the local Reynolds number.

3 Solution algorithm

In order to address the boundary value problems (10)-(12) which are accompanied by boundary conditions articulated in (13) and (14), we employed the bvp4c function, a pre-existing solver, within the MATLAB software package. The basis of the algorithm is established on a methodology that involves reducing the nonlinear ordinary differential equations (10)-(12) in conjunction with the boundary conditions (13) and (14) via a process of diminution, resulting in a system of first order nonlinear differential equations as presented below.

$$\begin{aligned} f&=y_1,\ \ f'=y_2,\ \ f''=y_3,\\ g&=y_4,\ \ g'=y_5,\ \ \theta=y_6,\ \ \theta'=y_7 \end{aligned} \quad (18)$$

By means of similarity transformation, equations (10), (11), and (12) can be reduced to first-order ordinary differential equations.

$$y_1'=f'=y_2 \quad (19)$$

$$y_2'=f''=y_3 \quad (20)$$

$$y_3'=\frac{1}{\left(1+\frac{1}{\beta}\right)}\left[y_2^2-y_1y_2+(M+\Omega)y_2-A_1y_5\right] \quad (21)$$

$$y_4=g \quad (22)$$

$$y_3'=g'=y_5 \quad (23)$$

$$y_5'=\frac{1}{\lambda_0}\left[y_2y_4-y_1y_5+A_1B(2y_4+y_3)\right] \quad (24)$$

$$y_6=\theta \quad (25)$$

$$y_6'=\theta'=y_7 \quad (26)$$

$$y_7'=-\frac{1}{\left(R+\frac{1}{Pr}\right)}\left[y_1y_7+\Delta y_6\right] \quad (27)$$

The boundary conditions yield

$$y_2(0)=\varepsilon, y_4(0)=0, y_6(0)=0 \quad \text{at} \quad y=0 \quad (28)$$

$$y_2(\eta)\to 1, y_4(\eta)\to 0, y_6(\eta)\to 1 \quad \text{at} \quad \eta=\infty \quad (29)$$

The nonlinear differential equations (19)-(27) together with the boundary equations (28) and (29) described above have been resolved through the utilization of the embedded function bvp4c in the MATLAB software.

4 Results and Discussions

The Equations (10), (11), and (12), following their transformation, were subjected to numerical solutions through the bvp4c routine in MATLAB, along with due consideration of the boundary conditions (13) and (14). The results thus obtained were subsequently analyzed and presented in the form of graphs, which demonstrate the behavior of non-dimensional parameters such as $\beta, M, \Omega, \lambda_\theta, \Delta, R, Pr, A_1$, and B, in relation to the simulated fluid velocity, along with temperature and micro rotation profiles. These graphs are vividly depicted in Figures 2-4.

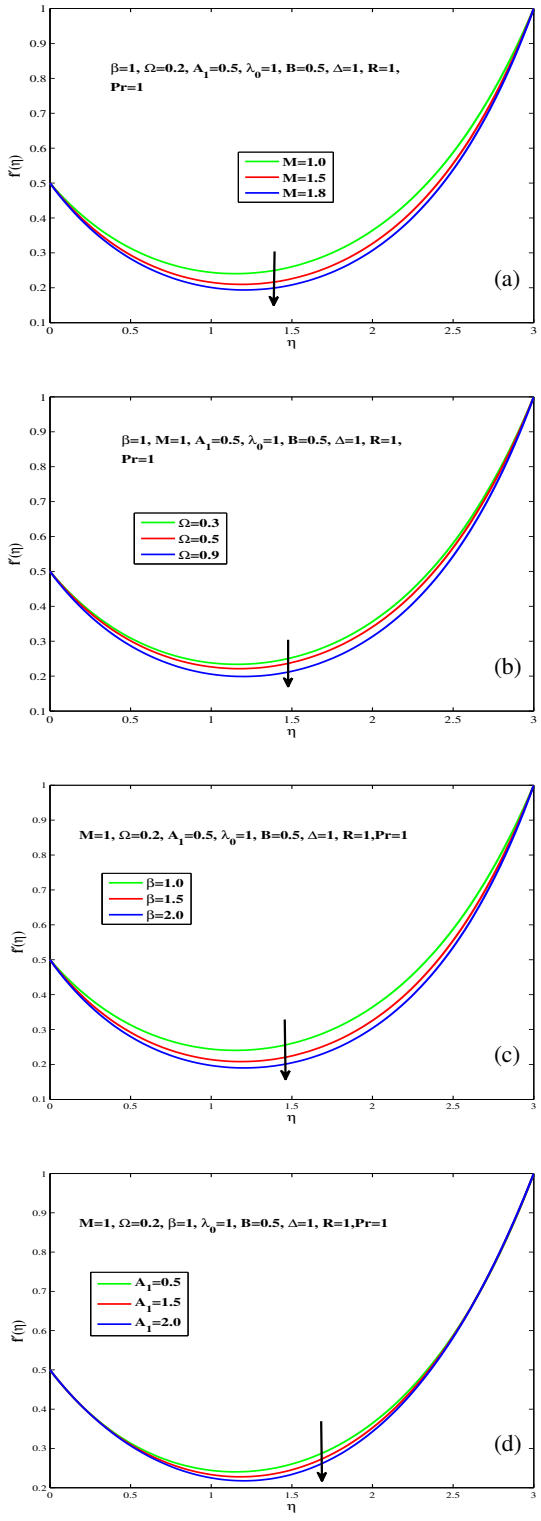

Fig. 2: Simulated velocity profile under the effect of the model parameters: (a) for various values of M, (b)for various values of permeability parameter, (c), for various values of β and (d) for varying values of micro-coupling parameter.

Figure 2(a) represents the effect of the M the velocity profile. On increasing the value of magnetic field parameter the velocity shows the decreasing behavior.

Figure 2(b) is the plot of various values of permeability parameter on velocity of the fluid. It's discovered that the velocity away from the stretching sheet is decreasing parabolically given a range of values permeability parameter.

Figure 2(c) show that the effect of Casson fluid parameter on simulated velocity. It raises the value of Casson fluid parameter then micropolar Casson fluid velocity down fall.

Figure 2(d) depict the impact of micro-coupling parameter on micropolar Casson fluid velocity. This plot clear that increases the value of micro-coupling parameter and the value of micropolar Casson fluid velocity decreases.

Table 1: Effects of various parameters on C_f

β	M	Ω	A_1	λ_0	B	Δ	R	Pr	$f''(0)$	$\mathscr{M}$
1.2	1	0.2	0.5	1	0.5	1	1	1	-0.5697	-1.0445
1.4	1	0.2	0.5	1	0.5	1	1	1	-0.5948	-1.0197
1.6	1	0.2	0.5	1	0.5	1	1	1	-0.6152	-0.9997
1	1.1	0.2	0.5	1	0.5	1	1	1	-0.5501	-1.1002
1	1.5	0.2	0.5	1	0.5	1	1	1	-0.5969	-1.1938
1	1.9	0.2	0.5	1	0.5	1	1	1	-0.6404	-1.2808
1	1	0.3	0.5	1	0.5	1	1	1	-0.5501	-1.1002
1	1	0.5	0.5	1	0.5	1	1	1	-0.5740	-1.1480
1	1	0.7	0.5	1	0.5	1	1	1	-0.5969	-1.1938
1	1	0.2	0.7	1	0.5	1	1	1	-0.5368	-1.0736
1	1	0.2	0.9	1	0.5	1	1	1	-0.5355	-1.0710
1	1	0.2	1.1	1	0.5	1	1	1	-0.5337	-1.0674
1	1	0.2	0.5	1.1	0.5	1	1	1	-0.5379	-1.0758
1	1	0.2	0.5	1.4	0.5	1	1	1	-0.5384	-1.0768
1	1	0.2	0.5	1.9	0.5	1	1	1	-0.5388	-1.0776
1	1	0.2	0.5	1	1.1	1	1	1	-0.5376	-1.0752
1	1	0.2	0.5	1	1.5	1	1	1	-0.5372	-1.0744
1	1	0.2	0.5	1	1.9	1	1	1	-0.5368	-1.0736
1	1	0.2	0.5	1	0.5	1.2	1	1	-0.5815	-1.1630
1	1	0.2	0.5	1	0.5	1.5	1	1	-0.6344	-1.2688
1	1	0.2	0.5	1	0.5	1.8	1	1	-0.6772	-1.3544
1	1	0.2	0.5	1	0.5	1	1.1	1	-0.5320	-1.0640
1	1	0.2	0.5	1	0.5	1	1.4	1	-0.5122	-1.0244
1	1	0.2	0.5	1	0.5	1	1.7	1	-0.4883	-0.9766
1	1	0.2	0.5	1	0.5	1	1	1.1	-0.5425	-1.0850
1	1	0.2	0.5	1	0.5	1	1	1.5	-0.5534	-1.1068
1	1	0.2	0.5	1	0.5	1	1	1.9	-0.5583	-1.5583

$$\mathscr{M} = Re_x^{1/2} C_f = \left(1 + \frac{1}{\beta}\right) f''(0)$$

Figure 3(a) portrays that the impact of λ_0 on Micro-rotation profile. On raising the value of spin gradient viscosity parameter, microelements seem to settle down up to $\eta = 1.788$, and beyond $\eta = 1.788$ they started rising.

Figure 3(b) portrays that the impact of micro-coupling parameter on micro-rotation profile. On raising the value of micro-coupling parameter, microelements seem to settle upward to $\eta = 1.273$, and beyond $\eta = 1.273$ they started downward.

Figure 3(c) shows that the effect of B on micro-rotation profile. On raising the value of micro-inertia density parameter, microelements seem to

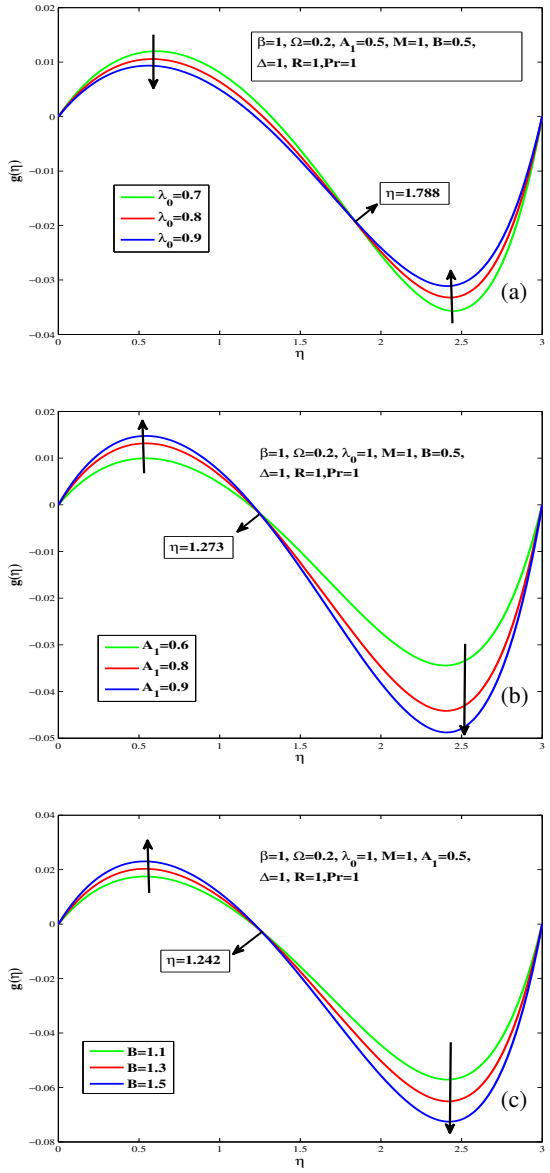

Fig. 3: Micro-rotation under the effect of the model parameters, (a) for various values of λ_0, (b) for varying values of A_1 , and (c) for various values of B.

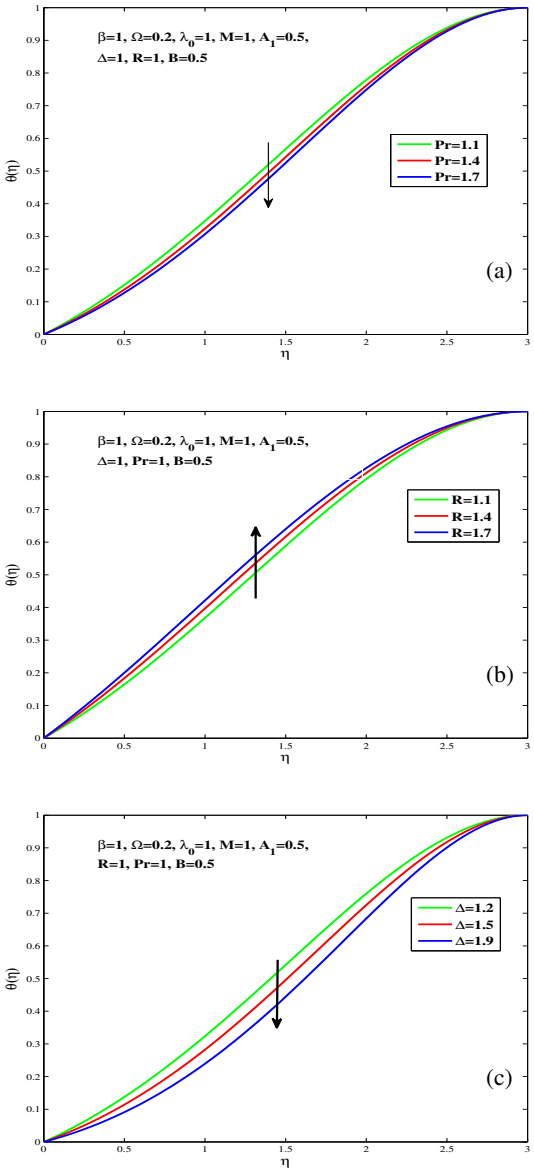

Fig. 4: Effect of model parameters on temperature profile, (a) Effect of Pr, (b) Effect of R, and (c) Effect of Δ.

settle upward to $\eta = 1.242$, and beyond $\eta = 1.242$ they started downward.

Figure 4(a) define clearly increase the value Prandtl number, the temperature profile decrease downward. Figure 4(b) As may be observed, the temperature profile increase, while fluid radiation parameter increases parabolic. Figure 4(c) as may be observed, Δ increases, temperature profile of the sheet decreases.

Table 1 illustrates the varying parameters' effects including the $\beta, \Omega, \lambda_0, \Delta, R, Pr, M, A_1$, and B, on the skin friction coefficient. Specifically, Table 1 demonstrates that a raise in the β, B, and R leads to a corresponding increase in the skin friction coefficient. Conversely, a raise in values of the$M, \Omega, \lambda_0, \Delta, B$, and Pr results in a decrease in the skin friction coefficient.

We observe that table 2 effects of different parameters like s $\lambda_0, M, \Omega, \beta, A_1, B, R, \Delta$ and Pr on Na_x. We noticed that increases the value M, Ω, β, A_1, B and R respectably, also decreases the value of Na_x. There is no effect of spin gradient parameter on Nusselt number. We investigate

increases the value of Δ and Pr, the Nusselt numbers also increase.

Table 2: Effect of different values β, M, Ω, A_1, λ_0, B, Δ, R and Pr on Na_x

β	M	Ω	A_1	λ_0	B	Δ	R	Pr	$f''(0)$	$\mathcal{N}$
1.0	1	0.2	0.5	1	0.5	1	1	1	0.2670	-0.5340
1.2	1	0.2	0.5	1	0.5	1	1	1	0.2692	-0.5384
1.6	1	0.2	0.5	1	0.5	1	1	1	0.2709	-0.5418
1	1.1	0.2	0.5	1	0.5	1	1	1	0.2679	-0.5358
1	1.5	0.2	0.5	1	0.5	1	1	1	0.2714	-0.5428
1	1.9	0.2	0.5	1	0.5	1	1	1	0.2745	-0.5490
1	1	0.3	0.5	1	0.5	1	1	1	0.2679	-0.5358
1	1	0.5	0.5	1	0.5	1	1	1	0.2706	-0.5412
1	1	0.9	0.5	1	0.5	1	1	1	0.2730	-0.5460
1	1	0.2	0.6	1	0.5	1	1	1	0.2671	-0.5342
1	1	0.2	0.9	1	0.5	1	1	1	0.2677	-0.5354
1	1	0.2	1.5	1	0.5	1	1	1	0.2694	-0.5388
1	1	0.2	0.5	1.1	0.5	1	1	1	0.2669	-0.5338
1	1	0.2	0.5	1.3	0.5	1	1	1	0.2669	-0.5338
1	1	0.2	0.5	1.5	0.5	1	1	1	0.2669	-0.5338
1	1	0.2	0.5	1	1.1	1	1	1	0.2670	-0.5340
1	1	0.2	0.5	1	1.4	1	1	1	0.2671	-0.5342
1	1	0.2	0.5	1	1.7	1	1	1	0.2672	-0.5344
1	1	0.2	0.5	1	0.5	1.1	1	1	0.2435	-0.4870
1	1	0.2	0.5	1	0.5	1.4	1	1	0.1891	-0.3782
1	1	0.2	0.5	1	0.5	1.8	1	1	0.1403	-0.2806
1	1	0.2	0.5	1	0.5	1	1.2	1	0.2969	-0.6532
1	1	0.2	0.5	1	0.5	1	1.6	1	0.3524	-0.7752
1	1	0.2	0.5	1	0.5	1	1.9	1	0.3905	-0.8591
1	1	0.2	0.5	1	0.5	1	1	1.2	0.2408	-0.4816
1	1	0.2	0.5	1	0.5	1	1	1.5	0.2135	-0.4270
1	1	0.2	0.5	1	0.5	1	1	1.8	0.1948	-0.3896

$\mathcal{N} = Re_x^{-1/2} Na_x = -(1+R)\,\theta'(0)$

5 Conclusions

- The simulative velocity of the sheet decreases when boost up the values of permeability parameter, magnetic parameter, Casson fluid parameter and micro-coupling parameter respectively.
- The parameters like Prandtl number and heat generation parameter have posited effect on temperature profile and found same effect of radiation parameter on temperature profile.
- On raising the value of spin gradient viscosity parameter, microelements seem to settle down up to $\eta = 1.788$, and beyond $\eta = 1.788$ they started rising.
- On raising the value of micro-coupling parameter, microelements seem to settle upward to $\eta = 1.273$, and beyond $\eta = 1.273$ they started downward.
- On raising the value of micro-inertia density parameter, microelements seem to settle upward to $\eta = 1.242$, and beyond $\eta = 1.242$ they started downward.
- Nusselt number shows directly proportional to Δ, Pr and inversely proportional to β, M, Ω, A_1, B, and R
- Skin friction shows same effect to β, A_1, R, and opposite effect to Δ, Pr, M, Ω, B, and λ_0.

Conflict of Interest

The authors declare that there is no conflict of interest regarding the publication of this paper.

Acknowledgment

TThis study is supported via funding from Prince Sattam bin Abdulaziz University project number (PSAU/2023/R/1444. The authors are thankful to the Deanship of Scientific Research at University of Bisha for supporting this work through the Fast-Track Research Support Program.

References

[1] A. C. Eringen, Simple microfluids, *International Journal of Engineering Science* **2**(2) (1964) 205–217.
[2] A. C. Eringen, Theory of micropolar fluids, *Journal of mathematics and Mechanics* (1966) 1–18.
[3] A. Borrelli, G. Giantesio and M. C. Patria, An exact solution for the 3d mhd stagnation-point flow of a micropolar fluid, *Communications in Nonlinear Science and Numerical Simulation* **20**(1) (2015) 121–135.
[4] H. Alkasasbeh, Numerical solution on heat transfer magnetohydrodynamic flow of micropolar casson fluid over a horizontal circular cylinder with thermal radiation, *Frontiers in Heat and Mass Transfer (FHMT)* **10** (2018).
[5] S. Pramanik, Casson fluid flow and heat transfer past an exponentially porous stretching surface in presence of thermal radiation, *Ain shams engineering journal* **5**(1) (2014) 205–212.
[6] N. Saidulu and A. V. Lakshmi, Mhd flow of casson fluid with slip effects over an exponentially porous stretching sheet in presence of thermal radiation, viscous dissipation and heat source/sink, *American Research J. of Mathematics* **2**(1) (2016) 1–15.
[7] J.-J. Shu, On micropolar fluid flow, *HEFAT 2011* (2011).
[8] A. D. Passos, V.-A. Chatzieleftheriou, A. A. Mouza and S. V. Paras, Casson fluid flow in a microchannel containing a flow disturbing rib, *Chemical Engineering Science* **148** (2016) 229–237.
[9] H. E. Hegab and G. Liu, Fluid flow modeling of micro-orifices using micropolar fluid theory, in *Microfluidic Devices and Systems III*, **4177**, SPIE2000, pp. 257–267.
[10] N. Mitarai, H. Hayakawa and H. Nakanishi, Collisional granular flow as a micropolar fluid, *Physical review letters* **88**(17) (2002) p. 174301.
[11] R. M. Ramana, K. V. Raju and J. G. Kumar, Multiple slips and heat source effects on mhd stagnation point flow of casson fluid over a stretching sheet in the presence of chemical reaction, *Materials Today: Proceedings* **49** (2022) 2306–2315.
[12] S. J. Reddy, P. Valsamy and D. S. Reddy, Radiation and heat source/sink effects on mhd casson fluid flow over a stretching sheet with slip conditions, *J. Math. Comput. Sci.* **11**(5) (2021) 6541–6556.

[13] P. Kumam, Z. Shah, W. Watthayu, T. Anwar *et al.*, Radiative mhd unsteady casson fluid flow with heat source/sink through a vertical channel suspended in porous medium subject to generalized boundary conditions, *Physica Scripta* **96**(7) (2021) p. 075213.
[14] S. U. Rehman, A. Mariam, A. Ullah, M. I. Asjad, M. Y. Bajuri, B. A. Pansera and A. Ahmadian, Numerical computation of buoyancy and radiation effects on mhd micropolar nanofluid flow over a stretching/shrinking sheet with heat source, *Case Studies in Thermal Engineering* **25** (2021) p. 100867.
[15] D. Dey, O. Makinde and R. Borah, Analysis of dual solutions in mhd fluid flow with heat and mass transfer past an exponentially shrinking/stretching surface in a porous medium, *International Journal of Applied and Computational Mathematics* **8**(2) (2022) p. 66.
[16] B. Saidulu and K. S. Reddy, Evaluation of combined heat and mass transfer in hydromagnetic micropolar flow along a stretching sheet when viscous dissipation and chemical reaction is present, *Partial Differential Equations in Applied Mathematics* **7** (2023) p. 100467.
[17] M. M. Nandeppanavar, R. Nagaraj and M. C. Kemparaju, Unsteady mhd stream of casson fluid over an elongating surface in the presence of thermal radiation and viscous dissipation, *Heat Transfer* **51**(6) (2022) 5159–5177.
[18] J. R. Howell, M. P. Mengüç, K. Daun and R. Siegel, *Thermal radiation heat transfer* (CRC press, 2020).
[19] T. Salahuddin and M. Awais, A comparative study of cross and carreau fluid models having variable fluid characteristics, *International Communications in Heat and Mass Transfer* **139** (2022) p. 106431.
[20] P. Jalili, H. Narimisa, B. Jalili, A. Shateri and D. Ganji, A novel analytical approach to micro-polar nanofluid thermal analysis in the presence of thermophoresis, brownian motion and hall currents, *Soft Computing* **27**(2) (2023) 677–689.
[21] P. Ganesan and G. Palani, Finite difference analysis of unsteady natural convection mhd flow past an inclined plate with variable surface heat and mass flux, *International journal of heat and mass transfer* **47**(19-20) (2004) 4449–4457.
[22] T. Hayat, M. I. Khan, M. Tamoor, M. Waqas and A. Alsaedi, Numerical simulation of heat transfer in mhd stagnation point flow of cross fluid model towards a stretched surface, *Results in physics* **7** (2017) 1824–1827.
[23] R. Djebali, F. Mebarek-Oudina and C. Rajashekhar, Similarity solution analysis of dynamic and thermal boundary layers: further formulation along a vertical flat plate, *Physica Scripta* **96**(8) (2021) p. 085206.
[24] A. Warke, K. Ramesh, F. Mebarek-Oudina and A. Abidi, Numerical investigation of the stagnation point flow of radiative magnetomicropolar liquid past a heated porous stretching sheet, *Journal of Thermal Analysis and Calorimetry* (2022) 1–12.
[25] K. Swain, F. Mebarek-Oudina and S. Abo-Dahab, Influence of mwcnt/fe 3 o 4 hybrid nanoparticles on an exponentially porous shrinking sheet with chemical reaction and slip boundary conditions, *Journal of Thermal Analysis and Calorimetry* **147**(2) (2022) 1561–1570.
[26] Z. Iqbal, R. Mehmood, E. Azhar and Z. Mehmood, Impact of inclined magnetic field on micropolar casson fluid using keller box algorithm, *The European Physical Journal Plus* **132** (2017) 1–13.
[27] A. R. M. Kasim, H. A. M. Al-Sharifi, N. S. Arifin, M. Z. Salleh and S. Shafie, Numerical solutions on boundary layer of casson micropolar fluid over a stretching surface, in *Proceedings of the Third International Conference on Computing, Mathematics and Statistics (iCMS2017) Transcending Boundaries, Embracing Multidisciplinary Diversities*, Springer2019, pp. 127–133.
[28] Z. Shah, A. Dawar, I. Khan, S. Islam, D. L. C. Ching and A. Z. Khan, Cattaneo-christov model for electrical magnetite micropoler casson ferrofluid over a stretching/shrinking sheet using effective thermal conductivity model, *Case Studies in Thermal Engineering* **13** (2019) p. 100352.
[29] H. T. Alkasasbeh, Numerical solution of micropolar casson fluid behaviour on steady mhd natural convective flow about a solid sphere, *Journal of Advanced Research in Fluid Mechanics and Thermal Sciences* **50**(1) (2018) 55–66.
[30] R. Jusoh and R. Nazar, Effect of heat generation on mixed convection of micropolar casson fluid over a stretching/shrinking sheet with suction, in *Journal of Physics: Conference Series*, **1212**(1), IOP Publishing2019, p. 012024.
[31] S. Rosseland, Astrophysik: Auf atomtheoretischer grundlage (1931).